Nanoscale Advances

ROYAL SOCIETY
OF CHEMISTRY

PAPER
Hiroshi Yukawa, Masazumi Fujiwara, Yoshinobu Baba *et al.*
A quantum thermometric sensing and analysis system using
fluorescent nanodiamonds for the evaluation of living stem
cell functions according to intracellular temperature

NCNST

PAPER

Check for updates

A quantum thermometric sensing and analysis system using fluorescent nanodiamonds for the evaluation of living stem cell functions according to intracellular temperature†

Hiroshi Yukawa, [ID] ‡*[abc] Masazumi Fujiwara, [ID] ‡*[d] Kaori Kobayashi,[b] Yuka Kumon,[b] Kazu Miyaji,[b] Yushi Nishimura,[cd] Keisuke Oshimi,[d] Yumi Umehara,[d] Yoshio Teki, [ID] [d] Takayuki Iwasaki,[e] Mutsuko Hatano,[e] Hideki Hashimoto[f] and Yoshinobu Baba*[abc]

Intracellular thermometry techniques play an important role in elucidating the relationship between the intracellular temperature and stem cell functions. However, there have been few reports on thermometry techniques that can detect the intracellular temperature of cells during several days of incubation. In this study, we developed a novel quantum thermometric sensing and analysis system (QTAS) using fluorescent nanodiamonds (FNDs). FNDs could label adipose tissue-derived stem cells (ASCs) at high efficiency with 24 h of incubation, and no cytotoxicity was observed in ASCs labeled with less than 500 µg mL^{-1} of FNDs. The peak of FNDs was confirmed at approximately 2.87 GHz with the characteristic fluorescence spectra of NV centers that could be optically detected (optically detected magnetic resonance [ODMR]). The ODMR peak clearly shifted to the high-frequency side as the temperature decreased and gave a mean temperature dependence of $-(77.6 \pm 11.0)$ kHz °C^{-1}, thus the intracellular temperature of living ASCs during several days of culturing could be precisely measured using the QTAS. Moreover, the intracellular temperature was found to influence the production of growth factors and the degree of differentiation into adipocytes and osteocytes. These data suggest that the QTAS can be used to investigate the relationship between intracellular temperature and cellular functions.

1. Introduction

Numerous types of stem cells, including induced pluripotent stem (iPS) cells, embryonic stem (ES) cells, and somatic stem cells, have been established, and their medical applications in regenerative medicine have been widely studied.[1–5] Somatic stem cells have already been confirmed to show great safety,

leading to various medical applications in regenerative medicine. In particular, adipose tissue-derived stem cells (ASCs) have recently attracted considerable attention as a multipotent stem cell source for regenerative medicine,[6,7] because large amounts of ASCs can be obtained using methods that are relatively easy to perform (*e.g.*, lipoaspiration under local anesthesia) and because ASCs are known to produce large amounts of growth factors (*e.g.*, hepatocyte growth factor [HGF] and vascular endothelial growth factor [VEGF]) in comparison to other somatic stem cells.[8–10] In addition, ASCs have the potential to self-renew and differentiate into many kinds of mesenchymal cells including adipocytes and osteocytes.

On the other hand, temperature is a very important parameter of the intracellular environment, since it can alter cell activities through the dynamics and reactivity of biomolecules. In recent years, the relationship between the temperature and the stem cell functions have been examined in a number of studies. Hossain *et al.* showed that mild heat exposure increased the proliferation of neural stem/progenitor cells (NCPCs) – possibly through the activation of the Akt pathway – and enhanced neuronal differentiation.[11] Eskander *et al.* showed that cold stimulation of stem cells of the apical papilla

[a]Institute of Nano-Life-Systems, Institutes of Innovation for Future Society, Nagoya University, Nagoya, Japan. E-mail: h.yukawa@nanobio.nagoya-u.ac.jp; babaymtt@chembio.nagoya-u.ac.jp

[b]Department of Biomolecular Engineering, Graduate School of Engineering, Nagoya University, Nagoya, Japan

[c]Institute of Quantum Life Science, National Institutes for Quantum and Radiological Science and Technology, Chiba, Japan

[d]Department of Chemistry, Graduate School of Science, Osaka City University, Osaka, Japan. E-mail: masazumi@osaka-cu.ac.jp

[e]Department of Electrical and Electronic Engineering, Graduate School of Engineering, Tokyo Institute of Technology, Tokyo, Japan

[f]School of Science and Technology, Kwansei Gakuin University, Hyogo, Japan

† Electronic supplementary information (ESI) available. See DOI: 10.1039/d0na00146e

‡ MT and HY contributed equally to the work presented here and should therefore be regarded as equivalent.

(SCAP) significantly increased the release of ATP ($p < 0.01$), and that the supernatant collected after cold stimulation of SCAP was able to activate cultured trigeminal neurons.[12] Velickovic *et al.* also showed that bone marrow-derived mesenchymal stem cells could be driven to form beige-like adipocytes *in vitro* by exposure to a reduced temperature.[13] However, the relationship between intracellular temperatures and stem cell functions remains unclear.

Intracellular thermometry techniques therefore play an important role in understanding the relationship between the intracellular temperature and stem cell conditions and functions. Various kinds of intracellular thermometry techniques have been reported, including thermo-sensitive fluorescent nanomaterials,[14] micro/nano-scale thermoelectric couples,[15] and infrared thermography.[16] Among these, techniques using thermo-sensitive fluorescent nanomaterials, including quantum dots (QDs), fluorescent nanodiamonds (FNDs), gold nanoclusters and polymer nanoparticles, have been the main intracellular thermometric techniques applied due to their non-invasiveness and high spatio-temporal properties in comparison to other techniques. However, there are few reports on thermometry techniques that can detect the intracellular temperature of stem cells during several days of incubation.

Thus, we focused on fluorescent quantum nanoparticles, such as QDs and FNDs, which have evolved to elucidate various biological activities both *in vivo* and *in vitro*.[17,18] Fluorescent quantum nanoparticles have excellent photostability with low cytotoxicity and have proven useful in biological imaging and nanoscale thermometry.[19–22] In particular, FNDs are expected to provide unprecedented temperature sensitivity by exploiting the coherent quantum properties of nitrogen vacancy (NV) centers. NV centers possess unpaired electron spins in diamond lattice structures that can be optically detected (optically detected magnetic resonance [ODMR]).[23–26] The frequency of the ODMR depends on the temperature, which thereby enables the measurement of nanoscale temperatures inside cells and tissues.

In this study, we developed a novel quantum thermometric sensing and analysis system (QTAS) by using FNDs that can detect the intracellular temperature of stem cells during several days of culturing and investigated whether the intracellular temperature influences the abilities of ASCs such as growth factor production and differentiation.

2. Methods

2.1. Quantum thermometry scheme

In-house-crafted cell culture dishes were made of plastic dishes with a glass bottom (coverslips) in which copper wires (diameter: 30 μm) were placed. The dishes were sanitized with a UV lamp before usage and then mounted on a three-axis scanning piezo stage of a home-built confocal fluorescence microscope. A continuous-wave 532 nm laser was used for excitation, with a typical excitation intensity of 4.7 W cm^{-2}. An oil-immersion microscope objective with a numerical aperture of 1.4 was used for both excitation and fluorescence collection. NV fluorescence was filtered using a dichroic beam splitter and a long-

pass filter to remove the residual green laser scattering. The microscope was then coupled to an optical fiber that acted as a pinhole (1550HP, core diameter approximately 10 μm; Thorlabs, USA). Fiber-coupled fluorescence was detected by an avalanche photodiode (SPCM AQRH-14; Excelitas, USA). Confocal fluorescence scanning images were obtained by scanning the sample with the piezo stage. Wide-field fluorescence images were obtained by switching the optical path to transfer images onto an EMCCD camera and defocusing the green excitation laser.

Microwaves were generated from a microwave source (SMB100A; Rohde & Schwarz, Germany) and amplified by 45 dB (ZHL-16W-43+; Mini-circuit, USA). The microwaves were fed to the microwave linear antenna (25 μm copper wire) in the in-house-crafted cell culture dishes. The typical microwave excitation power used for the continuous-wave ODMR spectral measurement under impedance mismatch conditions was 35 dBm (3.2 W). The magnetic field distribution of the input microwave was calculated by the finite-element method (COMSOL). The ODMR observable lower boundary of 5 A m^{-1} was determined by comparing the experimental results with the simulation data. Avalanche photodiode (APD) detection was gated for microwave irradiation ON and OFF using a radio-frequency (RF) switch (ZYSWA-2-50DRS; Mini-circuit) and a bit pattern generator (PBESR-PRO-300; Spincore, USA). The gate width of both gates was 200 μs. This was followed by an initialization time of 100 μs, giving I_{PL}^{ON} and I_{PL}^{OFF} with a repetition rate of 2 kHz. No external magnetic field was applied in this study.

The measurement accuracy of the FND thermometers on the coverslip and in air was evaluated as previously reported using

$$\delta T = \sqrt{\sum_{i=1}^{N}(T_i - T_{dish})^2/(N-1)}, \text{ where } T_i \text{ and } T_{dish} \text{ are the}$$

temperatures measured using the FND thermometers and the dish temperature, respectively.[21]

2.2. Materials

FNDs were purchased from Adámas Nanotechnologies (Raleigh, VA, USA). Dulbecco's modified Eagle's medium (DMEM)/F12 and Hank's balanced salt solution were purchased from Thermo Fisher Scientific K.K. (Tokyo, Japan). Fetal bovine serum (FBS) was purchased from Trace Scientific Ltd. (Melbourne, Australia). Collagenase Type I was purchased from Koken Co., Ltd. (Tokyo, Japan). A cell counting kit-8 (CCK-8) and Hoechst33342 solution were purchased from DOJINDO Laboratories (Kumamoto, Japan). ELISA kits for mouse HGF, TGF-β1, VEGF and EGF were purchased from R&D systems, Inc. (Minneapolis, USA). Adipo-Inducer Reagent and Osteoblast-Inducer Reagent were purchased from Takara Bio. Inc. (Shiga, Japan). Phycoerythrin (PE)-conjugated anti-mouse CD29 and CD105, lymphocyte antigen 6A/E (Ly-6A/E; also known as stem cell antigen-1 or Sca-1) antibodies, fluorescein isothiocyanate (FITC)-conjugated anti-mouse CD45, CD90, and CD117 antibodies, and allophycocyanin (APC)-conjugated anti-mouse CD44 antibodies were purchased from BD Biosciences (Tokyo, Japan).

2.3. Transmission electron microscopy

The samples were adsorbed onto carbon-coated copper grids (400 mesh) and stained with 2% phosphotungstic acid solution (pH 7.0) for 10 s. The grids were then observed using a transmission electron microscope (JEM-1400 Plus; JEOL Ltd., Tokyo, Japan) at an acceleration voltage of 80 kV. Digital images (3296 × 2472 pixels) were taken with a charge coupled device camera (EM-14830RUBY2, JEOL Ltd.).

2.4. Particle properties

The particle size and zeta potential distribution of FNDs in water were measured using a dynamic light-scattering spectrophotometer (ZETASIZER Nano-ZS; Malvern Instruments Ltd., Hyogo, Japan). The particle size and zeta potential were obtained from the peak of the size distribution graph. The absorbance spectra of FNDs were measured using an 8453A UV-visible spectrophotometer (Agilent Technology, Santa Clara, CA, USA). The fluorescence spectra were measured using a photonic multichannel analyzer (PMA-12; Hamamatsu Photonics, Shizuoka, Japan). The excitation wavelength was 558 nm.

2.5. Isolation and culture of ASCs

The methods used for the isolation and culture of ASCs have been reported previously.[10] In brief, 7 to 14 month-old female C57BL/6 mice were killed by cervical dislocation, and adipose tissue specimens were isolated from the inguinal groove and washed with Hank's buffer to remove blood cells. All animal procedures were performed in accordance with the Guidelines for Care and Use of Laboratory Animals of Nagoya University and approved by the Animal Ethics Committee of Nagoya University. The adipose tissues were cut finely and digested with type II collagenase at 37 °C in a shaking water bath for 90 min. Adipose tissue cells were suspended in cell culture medium (DMEM/F12 containing 20% FBS and 100 U mL^{-1} penicillin/streptomycin). The cells were centrifuged at 1200 rpm for 5 min at room temperature to obtain pellets containing the ASCs and then washed three times by suspension and centrifuged in the culture medium. The primary cells were cultured for 4–5 days until they reached confluence; this was defined as passage "0". Cells from passages 2–5 were used in all experiments.

2.6. Flow cytometry of ASCs

ASCs were incubated with antibodies for 30 min on ice. The antibodies used for detecting cell surface markers were as follows: phycoerythrin (PE)-conjugated anti-mouse CD29 (0.2 mg mL^{-1}) and CD105 (0.2 mg mL^{-1}), lymphocyte antigen 6A/E (Ly-6A/E; also known as stem cell antigen-1 or Sca-1; 0.2 mg mL^{-1}) antibodies, fluorescein isothiocyanate (FITC)-conjugated anti-mouse CD45 (0.5 mg mL^{-1}), CD90 (0.5 mg mL^{-1}), and CD117 antibodies (0.5 mg mL^{-1}) and allophycocyanin (APC)-conjugated anti-mouse CD44 antibodies (0.2 mg mL^{-1}). CD45 is a marker for pan-hematopoietic cells. CD29 (β1 integrin) and CD44 (phagocytic glycoprotein-1) are adhesion molecules and are used as markers for MSCs. CD90 (Thy-1) and CD105 (Endoglin) are markers for various stem cells, including MSCs. Flow cytometry was performed using a fluorescence activated cell sorter (FACS) (Calibur, BD Biosciences).

2.7. Transduction of FNDs into ASCs

ASCs were incubated with FNDs (250 μg mL^{-1}) in a transduction medium (DMEM/F12 containing 2% FBS and 100 U mL^{-1} penicillin/streptomycin) at 37 °C. After 24 h of incubation, the cells were washed 3 times using the transduction medium, and the nuclei of ASCs were then stained with Hoechst33342 solution. The red fluorescence derived from FNDs transduced into ASCs was observed by high-speed multiphoton confocal laser microscopy (A1MP+/A1RMP+; Nikon, Tokyo, Japan).

2.8. Observation of FND distribution in ASCs

To observe the distribution of FNDs in ASCs, ASCs were incubated at 37 °C on 35 mm glass bottomed dishes (Matsunami Glass Ind., Ltd., Osaka, Japan), and then FNDs (125 μg mL^{-1}) were added into the dishes. After 24 h of incubation, the ASCs were washed 3 times using the transduction medium, and the nuclei were stained with Hoechst33342. The two- and three-dimensional distribution of FNDs in ASCs was confirmed using a super-resolution structured illumination microscope (N-SIM; Nikon Co., Ltd.).

2.9. The cytotoxicity of FNDs to ASCs

ASCs (1 × 10^4 cells) were seeded in a 96-well plate (BD Falcon; BD Biosciences, Franklin Lakes, NJ, USA) with 100 μL of culture medium and then cultured for 24 h at 37 °C. FNDs were transduced into ASCs in transduction medium. After 24 h of incubation, the cells were washed 3 times with transduction medium. The viable cells were then counted using a cell counting kit-8 (CCK-8). CCK-8 reagent (10 μL) was added to each well, and the reaction was allowed to proceed for 2 h. The absorbance of the sample at 450 nm was measured against a background control using a microplate reader (Infinite® 200 PRO; Tecan Japan Co., Ltd., Kawasaki, Japan).

2.10. The proliferation of ASCs–FNDs

ASCs (4 × 10^3 cells) were seeded in a 96 well plate with 100 μL of culture medium for one day and then transduced with FNDs at various concentrations (0, 20, 50, 100, 500, and 750 μg mL^{-1}) for 24 h at 37 °C. ASCs labeled with FNDs (ASCs–FNDs) were washed three times with culture medium, and the medium was then replaced with 100 μL of new culture medium. After 2, 5, and 7 days, the viable cells were counted using CCK-8. The method was the same as that used to determine cytotoxicity.

2.11. Enzyme-linked immunosorbent assays

ASCs (2 × 10^5 cells) were seeded in a cell culture dish with 1 mL of culture medium overnight and then transduced with FNDs at a concentration of 5 μg mL^{-1} for 24 h at 37 °C. The ASCs–FNDs were washed three times with PBS, and then fresh transduction medium (1 mL) was added into the cell culture dish and the dish was incubated for 48 h (HGF, VEGF and epidermal growth factor [EGF]) or 96 h (transforming growth factor-β1 [TGF-β1]) at 32 °C, 37 °C and 42 °C. The culture supernatants were collected after incubation, and then the levels of mouse HGF, VEGF, TGF-

β1, and EGF produced by ASCs or ASCs–FNDs in the medium were measured using specific kits according to the manufacturers' protocols.

2.12. Adipogenic and osteogenic differentiation

Adipogenic differentiation was induced by culturing the cells for 3 days in DMEM (high glucose) containing 100 mM indometacin, 1 mM dexamethasone, 1 mM hydrocortisone, 10 mM insulin (I-5500; Sigma, Tokyo, Japan), and 10% FBS. The cells were then further cultured in DMEM (high glucose) containing 10% FBS for 2 weeks, and the medium was changed every 3 days. Differentiation was confirmed by conventional microscopic observation of intracellular lipid droplets. Oil Red O staining was used as an indicator of the intracellular lipid accumulation. Osteogenic differentiation was induced by culturing the cells for 2 weeks in DMEM containing 200 mM dexamethasone, 50 mM ascorbate-2-phosphate (013-12061; Wako Pure Chemical Industries Ltd., Tokyo, Japan), 10 mM α-glycerophosphate (G-9891; Sigma) and

10% FBS. Differentiation was confirmed by the staining of any alkaline phosphatase activity.

2.13. The statistical analysis of cell properties

Numerical values are presented as the mean ± standard error. Each experiment was repeated three times. Statistical significance was evaluated using an unpaired Student's *t*-test for comparisons between two groups; *P* values of <0.05 were considered to indicate statistical significance. All statistical analyses were performed using the SPSS software package.

3. Results

3.1. The experimental setup of a quantum thermometric sensing and analysis system (QTAS) for cultured cells

An illustration of the QTAS for cultured cells is shown in Fig. 1A. A real QTAS composed of an in-house-crafted cell culture dish with a heater and a three-axis scanning piezo stage of a confocal
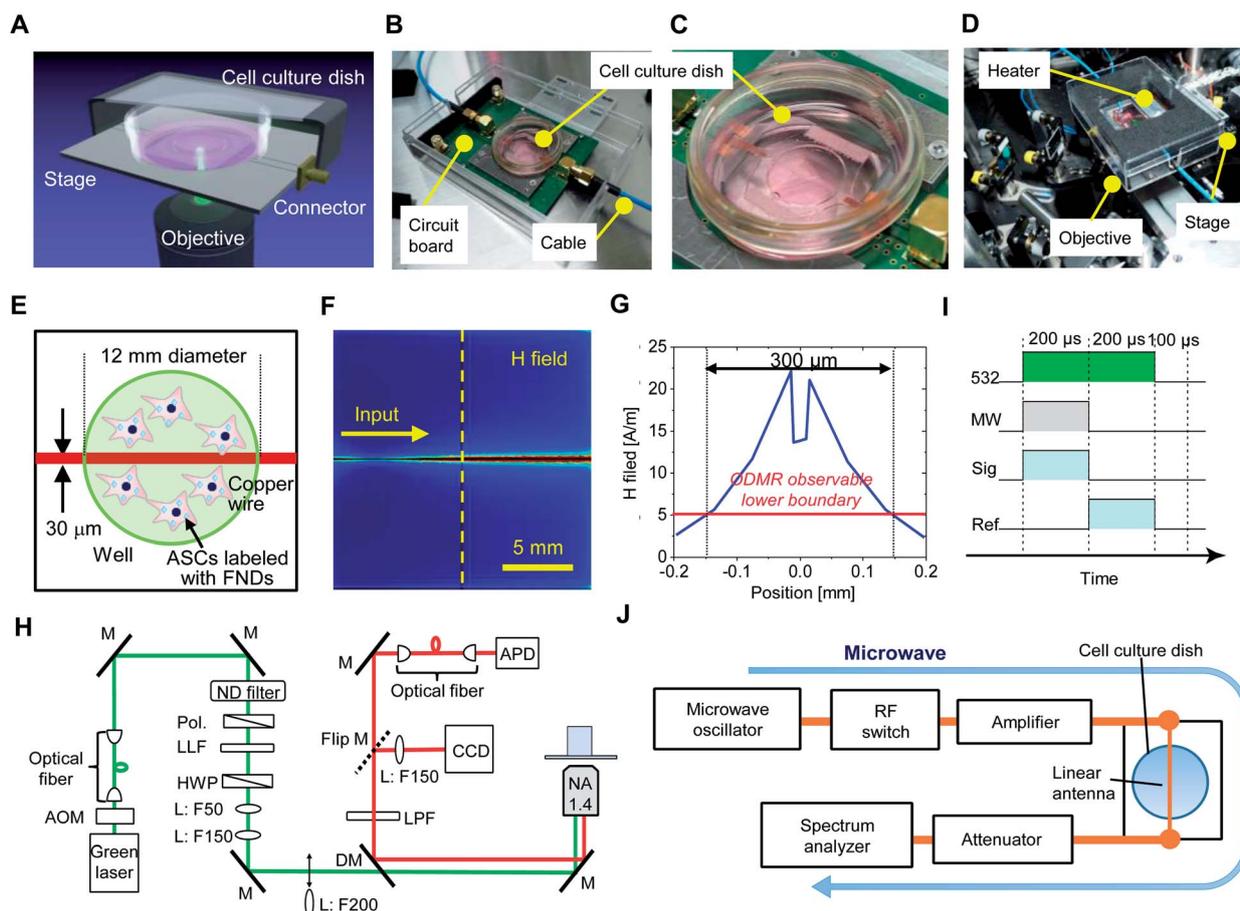

Fig. 1 The experimental setup of the quantum thermometric sensing and analysis system (QTAS) for cultured cells. (A) An illustration of the QTAS. (B) The three-axis scanning piezo stage of an in-house-crafted confocal fluorescence microscope. (C) An in-house-crafted cell culture dish composed of a plastic dish with a glass bottom (coverslip) and a copper wire (diameter: 30 μm) located between the plastic dish and coverslip. (D) A real QTAS composed of an in-house-crafted cell culture dish with a heater and the three-axis scanning piezo stage of an in-house-built confocal fluorescence microscope. (E) An image of cultured cells in the in-house-crafted cell culture dish. (F) The simulated magnetic field distribution on the dish. (G) 1D cross-sectional plot of the magnetic field along the yellow dashed line. (H) A schematic illustration of the optical setup of the confocal microscope. (I, J) A microwave circuit diagram (J) and the timing of the laser, microwave, and photon detection (I) of the QTAS.

fluorescence microscope that was built in house are shown in Fig. 1B–D. The cell culture dish (built in-house) was composed of a plastic dish with a glass bottom (coverslip) with a copper wire (diameter, 30 μm) located between the plastic dish and coverslip. ASCs could be incubated in our cell culture dish for several days. A schematic illustration of cells labeled with FNDs in the dish is shown in Fig. 1E. The magnetic field distribution on the dish and a cross-section of the area indicated with the vertical dashed line is shown in Fig. 1F. The area in which ODMR could be effectively performed was approximately 300 μm around the copper wire located in the center of the dish (Fig. 1G). A schematic diagram of the optical setup of the confocal microscope in the QTAS is shown in Fig. 1H. A microwave circuit diagram and the timing of the laser and microwave are shown in Fig. 1I, while the diagram for photon detection using the QTAS is shown in Fig. 1J.

3.2. Temperature stability of the QTAS

The temperature stability of the thermometry experiments was measured by placing a tiny thermocouple on the surface of the coverslips of the in-house-crafted cell culture dishes (Fig. 2A–D). The temporal temperature profiles for 35 min at 3 different set temperatures (36.6 °C, 37.9 °C, and 41.8 °C) are shown in Fig. 2A–C, respectively. A profile of the 12 h temperature stability at 41.8 °C is shown in Fig. 2D. These data suggested that the stability was ±0.1 °C for 30 min and ±0.2 °C for 12 h.

3.3. Operating principles of the QTAS by using fluorescent nanodiamonds (FNDs)

A schematic drawing of FNDs with NV centers in the diamond lattice structures is shown in Fig. 3A. The vacancy, carbon, nitrogen, and electrons in a FND are shown by light gray, dark
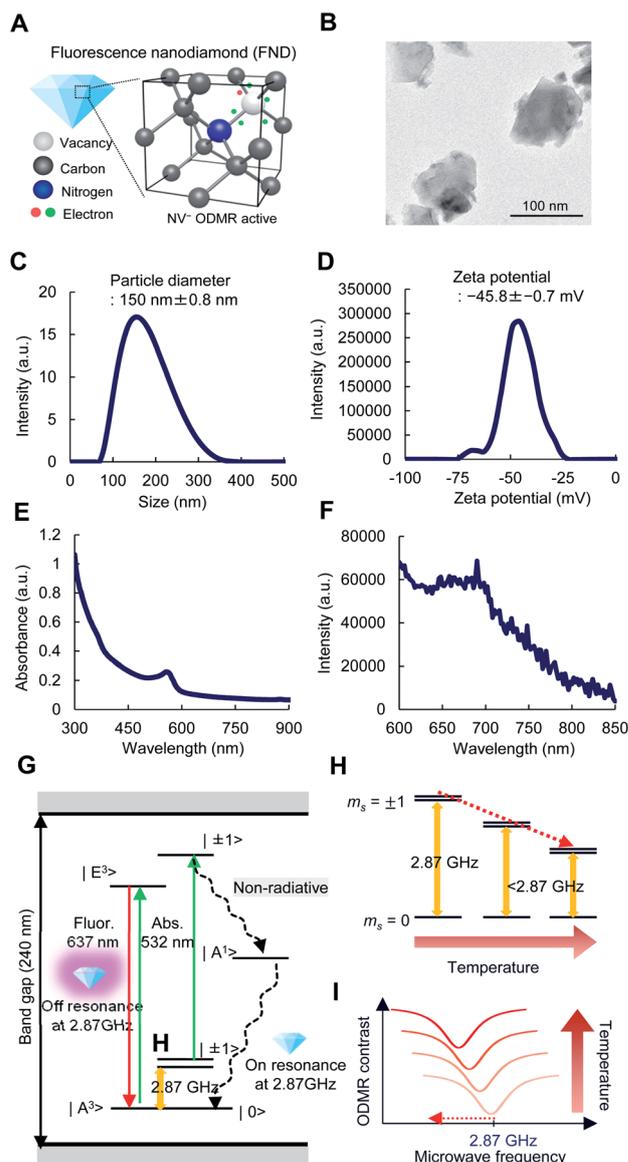

Fig. 2 The temperature stability of the thermometry experiments on the surface of coverslips of the in-house-crafted cell culture dishes by placing a tiny thermocouple. The temporal temperature profiles for 35 min at 3 different set temperatures (36.6 °C (A), 37.9 °C (B), and 41.8 °C (C)) were shown. A profile of the 12 h temperature stability at 41.8 °C was shown (D). The stability was ± 0.1 °C for 30 min and ±0.2 °C for 12 h.

Fig. 3 Schematic illustration of FND-based quantum thermometry. (A) An illustration of the crystal structure of negatively charged NV centers (NV⁻) that are ODMR-active. (B) A transmission electron micrograph of FNDs. (C) The size of FNDs. The average diameter of FNDs was 150 ± 0.8 nm (range: 80 to 300 nm). (D) The zeta potential of FNDs. The average zeta potential of FNDs was −45.8 ± 0.7 mV (range: −75 to −25 mV). (E, F) The absorbance (E) and fluorescence (F) spectra of FNDs in water. (G) A diagram of the energy levels of NV centers. The green, red, yellow sinusoidal, and black dashed sinusoidal arrows represent optical excitation, fluorescence emission, microwave excitation and intersystem crossing relaxation, respectively. (H, I) Schematic illustrations of the temperature dependence of the ODMR spectra. The fluorescence intensity of FNDs is decreased when the electron-spin-resonant is irradiated by microwaves at approximately 2.87 GHz (H). The ODMR peak is shifted to the lower frequency side as the temperature increases (I).
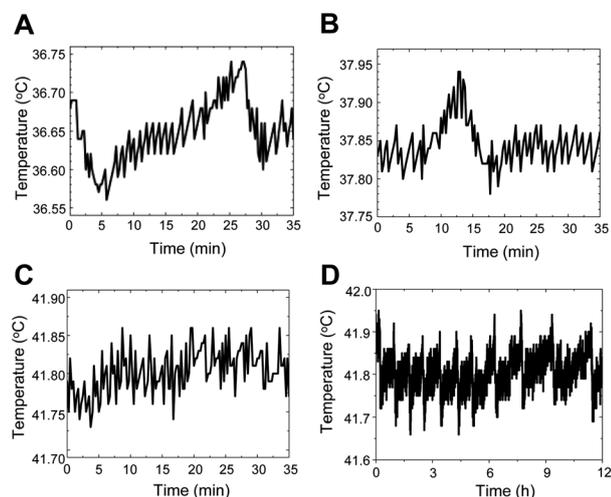
gray, blue, and red or green circles, respectively. An image of FNDs under a transmission electron microscope (TEM) is shown in Fig. 3B. FNDs had a rock-like shape, with an average diameter of 150 ± 0.8 nm (range, 80–330 nm) (Fig. 3C). The average zeta potential of FNDs was −45.8 ± 0.7 mV (range, −75

to −25 mV) (Fig. 3D). The absorbance and fluorescence spectra of FNDs in water are shown in Fig. 3E and F. Each FND particle contained approximately 500 NV centers.

NV centers have a spin-triplet electronic ground state with a long electron spin coherence time.[23] NV centers deeply create defect states, denoted as $|\vdash A^3\rangle$ and $|\vdash E^3\rangle$ for the ground and excited states, respectively, in a diamond band gap of 5.1 eV (roughly 240 nm) (Fig. 3G). Optical transitions between these two states absorb 532 nm green laser light and emit red-shifted fluorescence in the range of 630–750 nm with a zero-phonon line of 637 nm. The $|\vdash A^3\rangle$ state has magnetic sublevels of $|0,\vdash \pm1\rangle$ with zero-field splitting of 2.87 GHz. There is a non-radiative intersystem crossing between $|E^3,\vdash \pm1\rangle$ and the metastable singlet state $|\vdash A^1\rangle$. In the resonance induced by microwave excitation at 2.87 GHz, a fraction of the electrons is non-radiatively decayed to $|A^3,\vdash 0\rangle$. Thus, the change in the fluorescence between $|\vdash A^3\rangle$ and $|\vdash E^3\rangle$ can be detected when the microwave frequency is resonant to this zero-field splitting. The zero-field splitting has a temperature dependence due to the thermal expansion of the lattice structures and provides local temperature information (Fig. 3H and I). The local temperature of ASCs was measured by measuring the frequency shift of the ODMR peak of the FNDs.

3.4. Calibration of the QTAS by using FNDs

To calibrate the temperature response of the QTAS, FNDs were spin-coated on the surface of the glass bottom (coverslip) in a cell culture dish, and their ODMR and fluorescence spectra were measured at 40.9 °C (without cell culture medium) (Fig. 4A–D). A doubly split ODMR peak of FNDs was confirmed at approximately 2.87 GHz (Fig. 4A) with characteristic fluorescence spectra of NV centers (Fig. 4B). The temperature of the glass bottom spin-coated with FNDs in the cell culture dish was

then varied from 40.9 °C to 29.1 °C (Fig. 4C). The ODMR peak clearly shifted to the high-frequency side as the temperature decreased. These temperature-dependent measurements were performed for multiple FNDs ($n = 15$) to calibrate the frequency shift of the ODMR of the FND quantum thermometers (Fig. 4D). The solid line and the associated shaded areas were linearly fitted to the data and the 95% confidence interval, which gives a mean temperature dependence of $-(77.6 \pm 11.0)$ kHz °C^{-1} in close agreement with that reported previously.[27]

The ODMR measurements took 3–6 min depending on the measurement parameters, such as the number of accumulations, frequency resolutions and frequency sweep range. The temperature-induced fluctuation of the ODMR peak position during the measurement was therefore estimated to be approximately 3.5 kHz, an order of magnitude smaller than the present accuracy of quantum thermometry. Note that the pH and ionic strength had no significant effect on the ODMR peak shift, as confirmed previously.[28]

3.5. Introduction of FNDs into ASCs

ASCs (CD29$^+$, CD44$^+$, CD90$^+$, CD105$^+$, Sca-1$^+$, CD45$^-$, CD73$^-$, and CD117$^-$) were incubated with FNDs (125 µg mL^{-1}) for 24 h and then observed using super-resolution structured illumination microscopy. The red fluorescence derived from FNDs was observed in the ASCs (Fig. 5A and B). Three-dimensional images were observed to further investigate the distribution of FNDs in ASCs. FNDs were widely distributed in ASCs, but none were observed in the nucleus of ASCs (Fig. 5C and D). In addition, almost all ASCs were able to be labeled with FNDs with high efficiency (Fig. S1A–D†), and FNDs were mainly introduced into ASCs *via* micropinocytosis in the endocytosis pathway.

3.6. Cytotoxicity of FNDs to ASCs and the differentiation ability of ASCs–FNDs

To examine the cytotoxicity of FNDs to ASCs, various concentrations (0, 20, 50, 100, 500, and 750 µg mL^{-1}) of FNDs were transduced into ASCs for 24 h at 37 °C. More than 95% of the ASCs were observed to be alive at FND concentrations of ≤500 µg mL^{-1}. Significant cytotoxicity was confirmed in ASCs transduced with 750 µg mL^{-1} of FNDs, and >75% of the cells were dead (Fig. 5E). The influence of FNDs on the proliferation rate of ASCs was also investigated within the non-cytotoxic range of concentrations. ASCs labeled with FNDs (ASCs–FNDs) exhibited a growth rate that was nearly equal to that of normal (non-labeled) ASCs. There were no significant differences in the proliferation of ASCs at these concentrations (Fig. 5F). These data suggest that ASCs can be labeled with FNDs at concentrations of ≤500 µg mL^{-1}.

In addition, to examine the influence of FNDs (125 µg mL^{-1}) on the differentiation ability of ASCs into adipocytes and osteocytes, normal ASCs (control) and ASCs–FNDs were differentiated into adipocytes and osteoblasts. The differentiation abilities of ASCs–FNDs into both adipocytes and osteoblasts were similar to those of normal ASCs (Fig. S2A and B†). These data suggest that FNDs (<250 µg mL^{-1}) do not affect the differentiation of ASCs into adipocytes and osteocytes.
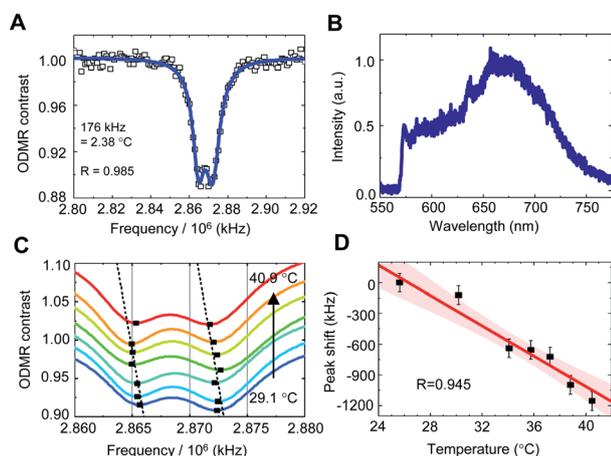

Fig. 4 Calibration of the ODMR peak shift of FNDs in the QTAS. (A) Typical ODMR spectrum of a single FND measured at 40.9 °C. (B) The fluorescence spectrum of this FND. (C) A close-up of the ODMR peaks of this FND at temperatures from 29.1 °C to 40.9 °C. The dashed lines were linearly fitted to the positions of the peaks. (D) The ODMR peak shifted to the high-frequency side as the temperature decreased. The solid line and the associated shaded area are the linear fit and the 95% confidence intervals. The data are shown as mean ± SD values.
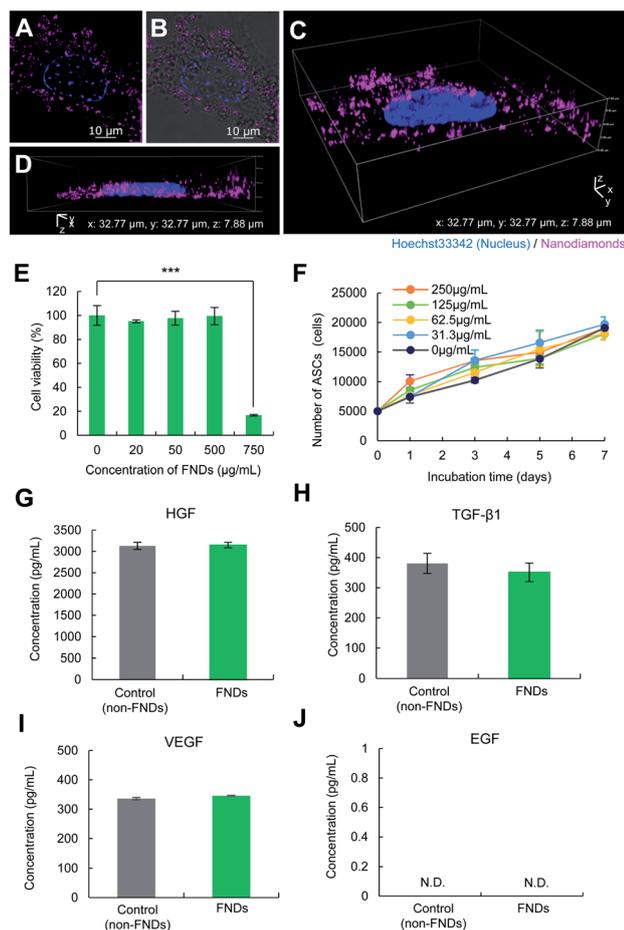
Fig. 5 Influence of FND labeling of ASCs. (A–D) Two- and three-dimensional fluorescence images of ASCs labeled with FNDs (ASCs–FNDs). Two-dimensional fluorescence images (A), a merged image (bright field and fluorescence images) (B) and three-dimensional fluorescence images (C, D). (E) The viability of ASCs–FNDs at different concentrations of FNDs. (F) The proliferation rate of ASCs–FNDs with non-cytotoxic concentrations of FNDs. (G, H) The comparison of the production of growth factors (HGF [G], VEGF [H], TGF-β1 [I], and EGF [J]) between ASCs (non-labeled) and ASCs–FNDs. The data are shown as mean ± SD values. ***$p < 0.001$.

3.7. Influence of FNDs on the stem cell ability of ASCs

ASCs have an important ability to produce growth factors such as HGF, TGF-β1, VEGF and EGF in regenerative medicine. To confirm the influence of FNDs on the production of growth factors from ASCs–FNDs, the HGF (Fig. 5G), TGF-β1 (Fig. 5H), VEGF (Fig. 5I), and EGF (Fig. 5J) levels in the supernatant of the culture medium, the ASCs of which were incubated for 48 h or 96 h, were measured using each ELISA kit. The production of HGF, TGF-β1 and VEGF from ASCs–FNDs could be confirmed, and the levels were maintained at the same level as that from non-labeled ASCs (control). On the other hand, the production of EGF could not be confirmed in either normal ASCs (control) or ASCs–FNDs. Moreover, to confirm the influence of FNDs on the differentiation ability of ASCs, ASCs–FNDs were differentiated into adipocytes and osteocytes at 37 °C. ASCs–FNDs could be confirmed to differentiate into adipocytes and osteocytes. These data suggested that FNDs do not affect the stem cell

functions of ASCs such as growth factor production and differentiation.

3.8. Detection of the intracellular temperature of living ASCs–FNDs using the QTAS

A schematic diagram of the measurement of the intracellular temperature of living ASCs–FNDs using the QTAS is shown in Fig. 6A. The changes of the intracellular temperature of living ASCs could be detected by the QTAS during several days of incubation. Two types of microscope images (white-light illumination with FND fluorescence and FND fluorescence alone) of living ASCs–FNDs in the cell culture dish are shown in Fig. 6B and C. A few FNDs near the nucleus could be observed. The corresponding confocal fluorescence scanning micrograph of the box ($16 \times 16 \ \mu m^2$) in Fig. 6C is shown in Fig. 6D. Yellow arrows indicate the FNDs in ASCs, and the fluorescence derived from FNDs in ASCs could be observed (Fig. 6D). The ODMR spectrum of FNDs in living ASCs (indicated by an arrow in Fig. 6D) at 40.9 °C was measured (Fig. 6E). This FND showed a sharp ODMR peak profile, and the ODMR peak was fitted with a two-peak Lorentzian profile to determine the position of the peak. When the dish temperature was then varied between 24.0 °C and 40.9 °C, a plot of the ODMR peak shift as a function of temperature was obtained (Fig. 6F). Linear fitting to the data with an experimentally determined slope of $-(77.6 \pm 11.0)$ kHz °C^{-1} (Fig. 4D) was carried out, which shows good agreement with $R^2 = 0.94$. The accuracy was ±79.4 kHz (±1.0 °C). In addition, the changes in the intracellular temperature of fixed ASCs could be detected using the QTAS (Fig. S3†). The sensitivity of the QTAS was 2.2 °C/$\sqrt{\text{Hz}}$ by considering the linewidth, ODMR contrast and photon counts to be 12.1 MHz, 0.05 and 2 Mcps, respectively.[29] This sensitivity is comparable to previous reports based on the same whole-spectrum method.[22] These data showed that the QTAS successfully detected continuous temperature changes in living stem cells. Note that the FND concentration of 5 μg mL^{-1} was used for labeling ASCs in this experiment to facilitate tracking the same FND for a long time.

3.9. Influence of intracellular temperature on the stem cell abilities of ASCs

To confirm the influence of the intracellular temperature on the production ability of growth factors from ASCs, the levels of HGF, TGF-β1, VEGF and EGF in the culture medium after ASC incubation were measured using appropriate ELISA kits (Fig. 6G–N). The levels of HGF (Fig. 6G), TGF-β1 (Fig. 6H) and VEGF (Fig. 6I) from ASCs at 32 °C were significantly lower than those at 37 °C. On the other hand, the levels of HGF (Fig. 6K) with a significant difference and TGF-β1 (Fig. 6L) at 42 °C were lower than those at 37 °C, while the level of VEGF (Fig. 6M) at 42 °C was significantly higher than that at 37 °C. On the other hand, the production of EGF (Fig. 6J and N) from ASCs could not be detected under any of the temperature conditions. Moreover, to confirm the influence of intracellular temperature on the differentiation ability of ASCs, ASCs were differentiated into adipocytes and osteocytes at 32 °C and 42 °C for 2 weeks.
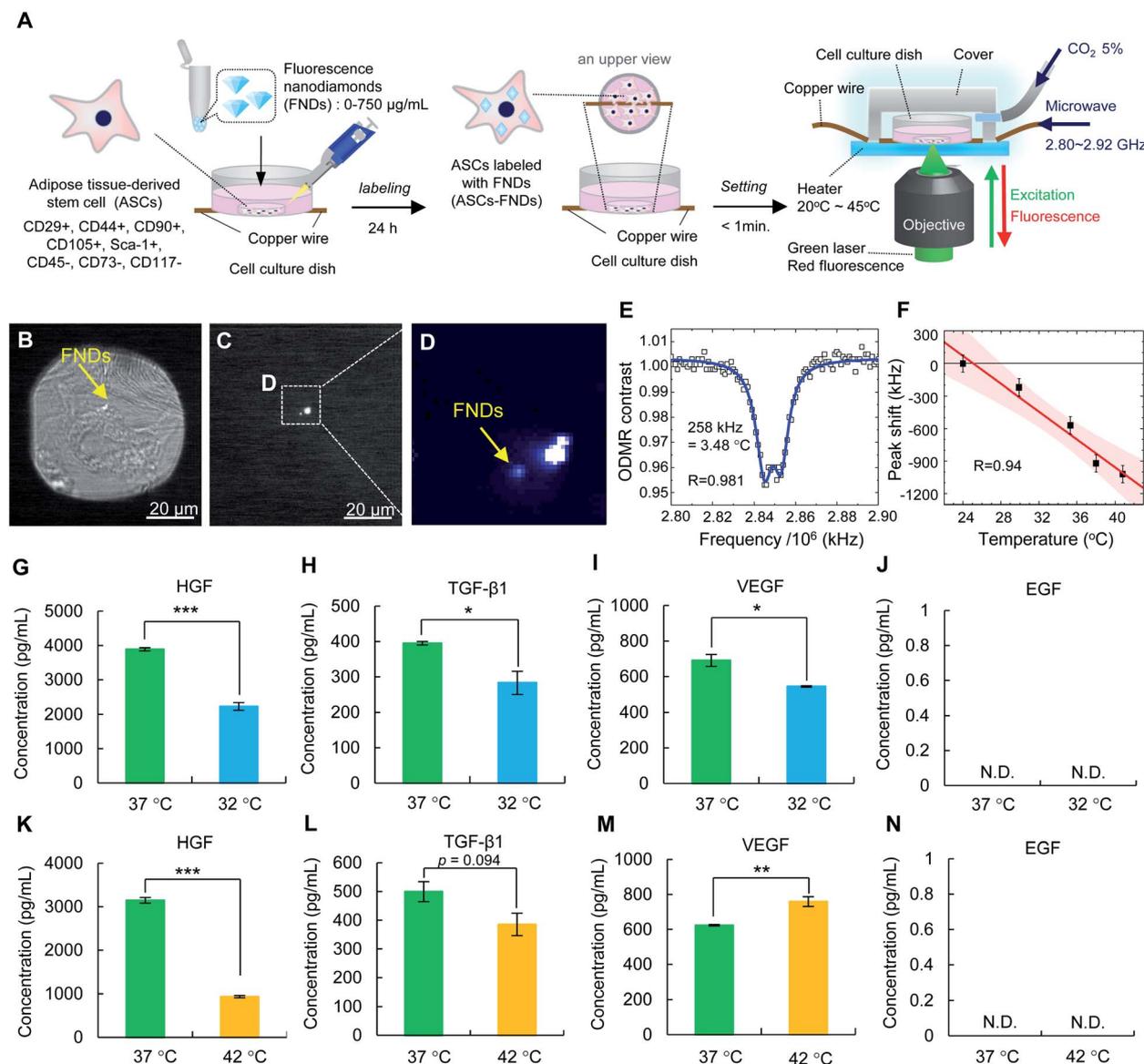
Fig. 6 Detection of the temperature change inside living ASCs–FNDs using the QTAS. (A) A schematic diagram of the measurement of the temperature change inside living ASCs–FNDs using the QTAS. (B, C) Two types of micrographs of living ASCs–FNDs in an in-house-crafted cell culture dish: white-light illumination with FND fluorescence (B) and FND fluorescence alone (white-light off) (C). (D) Confocal fluorescence scanning image of the small box in (C). (E) The ODMR spectrum of the FND indicated by a yellow arrow in (D) at 40.8 °C with fitted functions. (F) The observed peak shifts as a function of the dish temperatures. The solid line and the associated shaded area are the linear fit and 95% confidence interval. (G–J) The comparison of the production of growth factors (HGF [G], VEGF [H], TGF-β1 [I], and EGF [J]) by ASCs–FNDs between at 37 °C and 42 °C. (K–N) The comparison of the production of growth factors (HGF [K], VEGF [L], TGF-β1 [M], and EGF [N]) by ASCs–FNDs between at 37 °C and 32 °C. The data are shown as mean ± SD values. *$p < 0.05$, **$p < 0.01$, ***$p < 0.001$.

ASCs could not survive and differentiate into adipocytes and osteocytes at either 32 °C or 42 °C (data not shown). These data suggested that intracellular temperature may affect the stem cell functions of ASCs, such as their production of growth factors and differentiation ability.

4. Discussion

In regenerative medicine, the development of an intracellular thermometry technique for measuring the temperature of living cells during several days of incubation is necessary for understanding the relationship between intracellular temperature and stem cell functions, because the temperature is not spatially uniform in realistic situations of stem cell transplantation. However, there are few reports on thermometry techniques can detect intercellular temperature during several days of incubation. We developed a novel QTAS for this purpose. The in-house-crafted cell culture dish used in the QTAS was designed based on a 35 mm glass bottomed dish. Coating the surface of the glass bottom with substances such as fibronectin and gelatin was easy; thus, sensitive cells, including stem cells, could be incubated in this in-house-crafted cell

culture dish with high versatility. In addition, an in-house-built confocal fluorescence microscope was incorporated in the QTAS, so the morphology of living cells could be observed in real time. On the other hand, living cells around the copper wire located in the cell culture dish could be programmatically irradiated with microwaves. At present microwave irradiation can only be performed around the linear microwave antenna. The irradiation area could be increased up to several square millimeters by employing loop gap antenna structures. Thus, the QTAS using FNDs was expected to be serve as a novel quantum intracellular thermometry system.

We focused on FNDs as fluorescence quantum nanoparticles, because of their excellent photostability, low cytotoxicity and ODMR activity. The FNDs used in this study contained approximately 500 NV centers and the diameter was from approximately 80 nm to 330 nm; thus, the FNDs could be introduced into stem cells with low cytotoxicity and detect the intracellular temperature of the cells. However, the shapes of the ODMR spectra of FNDs were found to be heterogeneous, as shown in Fig. 4A. The spectral shape of the ODMR peak affects the precision of thermometry. The double-peak structure in the ODMR spectra could not be perfectly reproduced by the two-peak Lorentzian profiles; thus, it was difficult to determine the peak position with high accuracy. We instead measured the ODMR peak shift dependent on temperature in the broad range of 24–40 °C, and achieved a thermometer accuracy of ±1.0 °C. If the ODMR peak did not have a peak split, then the same level of accuracy could be obtained with a higher precision of ±0.5 °C. This also highlights the importance of the uniformity of the spin properties of the NV centers for material development studies related to FNDs. In addition, while the FND used in Fig. 6 exhibited a temperature dependence of the zero-field splitting close to the previous value of -74 kHz K^{-1}, there exists a significant variation of the temperature dependency among FNDs.[30] This can be, in principle, resolved by calibrating the temperature dependency of each ND in advance of the temperature measurements.

In addition to bone marrow stem cells (BMSCs), ASCs are widely used in clinical practice and have already been reported to secrete a large amounts of growth factors such as HGF and VEGF. We therefore evaluated the relationship between the intracellular temperature and the functions of ASCs. FNDs could label ASCs at high efficiency with low cytotoxicity and wide distribution. In addition, FNDs did not affect the abilities of ASCs, which include cellular proliferation, growth factor production (HGF, VEGF and TGF-β1) and differentiation; thus, FNDs could be applied to the quantum intracellular thermometry of ASCs. These results are consistent with those in previous studies.[31–33] Other fluorescence nanomaterials that can measure intracellular temperature, such as fluorescence proteins[34–36] and fluorescence polymer nanoparticles,[37,38] have also been developed. However, they are limited in terms of their photostability and cytotoxicity. In comparison to these probes, the present method using FNDs provides supreme photostability, even at the single-NV level, with very low cytotoxicity. The present FND quantum thermometry technique enables exploration in different fields of thermogenic events across a wide variety of biological targets for which organic probes cannot be used.

The QTAS enabled us to demonstrate quantum thermometry of ASCs by detecting the spectral peak shift of NV centers in FNDs on ODMR, which was dependent on the intracellular temperature. In this study, the levels of growth factor production (HGF, VEGF and TGF-β1) were found to be significantly changed by the intracellular temperature. Transient receptor potential (TRP) channels, which respond to physical stimuli (temperature, osmotic pressure, and mechanical stimulation) and which exchange intracellular signals, are considered to be thermometric sensors in cells. At present, the TRP channels are known to influence the proliferation, differentiation and death mechanism of various types of cells. TRPV1, TRPM2 and TRPV8 in TRP channels, which can detect temperatures of 42 °C and 37 °C, were found to be expressed on ASCs (data not shown); thus, the intracellular temperature was assumed to influence the growth factor production through these TRP channels. In addition to ASCs, this QTAS can be applied to other types of cells, such as other stem cells, cancer cells, normal cells and organoids, and is therefore expected to contribute to the elucidation of the relationship between intracellular temperatures and cell functions.[39,40]

5. Conclusions

We developed a novel QTAS using FNDs in order to elucidate the relationship between intracellular temperature and stem cell functions. ASCs could be labeled with FNDs at high efficiency with 24 h of incubation, and no cytotoxicity was observed in ASCs labeled with <500 μg mL^{-1} of FNDs. The peak of FNDs could be confirmed at approximately 2.87 GHz with characteristic fluorescence spectra of NV centers that could be optically detected by ODMR. The ODMR peak clearly shifted to the high-frequency side as the temperature decreased, showing a mean temperature dependence of $-(77.6 \pm 11.0)$ kHz °C^{-1}; thus in living ASCs, intracellular temperatures between 24.0 °C and 40.9 °C could be precisely measured using the QTAS during several days of culturing. Moreover, the intracellular temperature was found to influence the production of growth factors (HGF, TGF-β1 and VEGF) and the degree of differentiation into adipocytes and osteocytes. These data suggest that the QTAS could be used for the precise measurement of the intracellular temperature of living stem cells and that it would be useful for elucidating the relationship between the intracellular temperature and the stem cell functions of ASCs.

Conflicts of interest

There are no conflicts to declare.

Acknowledgements

References

1 Y. Shi, H. Inoue, J. C. Wu and S. Yamanaka, *Nat. Rev. Drug Discovery*, 2017, **16**, 115–130.

2 M. Nakagawa, M. Koyanagi, K. Tanabe, K. Takahashi, T. Ichisaka, T. Aoi, K. Okita, Y. Mochiduki, N. Takizawa and S. Yamanaka, *Nat. Biotechnol.*, 2008, **26**, 101–106.

3 J. Andersen and S. P. Paşca, *Nature*, 2018, **563**, 44–45.

4 L. Beccari, N. Moris, M. Girgin, D. A. Turner, P. Baillie-Johnson, A. C. Cossy, M. P. Lutolf, D. Duboule and A. M. Arias, *Nature*, 2018, **562**, 272–276.

5 Y. Mizunaga, S. Terai, N. Yamamoto, K. Uchida, T. Yamasaki, N. Nishina, Y. Fujita, K. Shinoda, Y. Hamamoto and I. Sakaida, *Cell Transplant.*, 2012, **21**, 2363–2375.

6 C. X. Zheng, B. D. Sui, N. Liu, C. H. Hu, T. He, X. Y. Zhang, P. Zhao, J. Chen, K. Xuan and Y. Jin, *Sci. Rep.*, 2018, **8**, 5215.

7 R. Doi, Y. Tsuchiya, N. Mitsutake, S. Nishimura, M. Matsuu-Matsuyama, Y. Nakazawa, T. Ogi, S. Akita, H. Yukawa, Y. Baba, N. Yamasaki, K. Matsumoto, T. Miyazaki, R. Kamohara, G. Hatachi, H. Sengyoku, H. Watanabe and T. Obata, *Sci. Rep.*, 2018, **7**, 8447.

8 D. Onoshima, H. Yukawa and Y. Baba, *Adv. Drug Delivery Rev.*, 2015, **95**, 2–14.

9 H. Yukawa, M. Watanabe, N. Kaji, Y. Okamoto, M. Tokeshi, Y. Miyamoto, N. Noguchi, Y. Baba and S. Hayashi, *Biomaterials*, 2012, **33**, 2177–2186.

10 H. Yukawa, Y. Kagami, M. Watanabe, K. Oishi, Y. Miyamoto, Y. Okamoto, M. Tokeshi, N. Kaji, H. Noguchi, K. Ono, M. Sawada, Y. Baba, N. Hamajima and S. Hayashi, Quantum dots labeling using octa-arginine peptides for imaging of adipose tissue-derived stem cells, *Biomaterials*, 2010, **31**, 4094–4103.

11 M. E. Hossain, K. Matsuzaki, M. Katakura, N. Sugimoto, A. A. Mamun, R. Islam, M. Hashimoto and O. Shido, *PLoS One*, 2017, **12**, e0190356.

12 M. A. Eskander, K. Takimoto and A. Diogenes, *Neuroscience*, 2017, **360**, 61–67.

13 K. Velickovic, H. A. Lugo Leija, I. Bloor, J. Law, H. Sacks, M. Symonds and V. Sottile, *Sci. Rep.*, 2018, **8**, 4974.

14 F. Vetrone, R. Naccache, A. Zamarrón, A. Juarranz de la Fuente, F. Sanz-Rodríguez, L. Martinez Maestro, E. Martín Rodriguez, D. Jaque, J. García Solé and J. A. Capobianco, *ACS Nano*, 2010, **4**, 3254–3258.

15 S. Sadat, A. Tan, Y. J. Chua and P. Reddy, *Nano Lett.*, 2010, **10**, 2613–2617.

16 R. Legrand, M. Abi Ghanem, L. Plawinski, M.-C. Durrieu, B. Audoin and T. Dehoux, *Appl. Phys. Lett.*, 2015, **107**, 263703.

17 W. W. Hsiao, Y. Y. Hui, P. C. Tsai and H. C. Chang, *Acc. Chem. Res.*, 2016, **49**, 400–407.

18 H. Yukawa and Y. Baba, *Anal. Chem.*, 2017, **89**, 2671–2681.

19 L. M. Maestro, E. M. Rodríguez, F. S. Rodríguez, M. C. la Cruz, A. Juarranz, R. Naccache, F. Vetrone, D. Jaque, J. A. Capobianco and J. G. Solé, *Nano Lett.*, 2010, **10**, 5109–5115.

20 R. Tanimoto, T. Hiraiwa, Y. Nakai, Y. Shindo, K. Oka, N. Hiroi and A. Funahashi, *Sci. Rep.*, 2016, **6**, 22071.

21 G. Kucsko, P. C. Maurer, N. Y. Yao, M. Kubo, H. J. Noh, P. K. Lo, H. Park and M. D. Lukin, *Nature*, 2013, **500**, 54–58.

22 D. A. Simpson, E. Morrisroe, J. M. McCoey, A. H. Lombard, D. C. Mendis, F. Treussart, L. T. Hall, S. Petrou and L. C. L. Hollenberg, *ACS Nano*, 2017, **11**, 12077–12086.

23 M. W. Doherty, N. B. Manson, P. Delaney, F. Jelezko, J. Wrachtrup and L. C. L. Hollenberga, *Phys. Rep.*, 2013, **528**, 1–45.

24 P. Neumann, I. Jakobi, F. Dolde, C. Burk, R. Reuter, G. Waldherr, J. Honert, T. Wolf, A. Brunner and J. H. Shim, *Nano Lett.*, 2013, **13**, 2738–2742.

25 M. Fujiwara, Y. Shikano, R. Tsukahara, S. Shikata and H. Hashimoto, *Sci. Rep.*, 2018, **8**, 14773.

26 M. Fujiwara, K. Yoshida, T. Noda, H. Takashima, A. W. Schell, N. Mizuochia and S. Takeuchi, *Nanotechnology*, 2016, **27**, 455202.

27 V. M. Acosta, E. Bauch, M. P. Ledbetter, A. Waxman, L. S. Bouchard and D. Budker, *Phys. Rev. Lett.*, 2010, **104**, 070801.

28 M. Fujiwara, R. Tsukahara, Y. Sera, H. Yukawa, Y. Baba, S. Shibata and H. Hashimoto, *RSC Adv.*, 2019, **9**, 12606.

29 G. Q. Liu, X. Feng, N. Wang, Q. Li and R. B. Liu, *Nat. Commun.*, 2019, **10**, 1344.

30 C. Foy, L. Zhang, M. E. Trusheim, K. R. Bagnall, M. Walsh, E. N. Wang and D. R. Englund, 2020, arXiv:1903.05717.

31 S. P. Blaber, C. J. Hill, R. A. Webster, J. M. Say, L. J. Brown, S. C. Wang, G. Vesey and B. R. Herbert, *PLoS One*, 2013, **8**, e52997.

32 T. C. Hsu, K. K. Liu, H. C. Chang, E. Hwang and J. I. Chao, *Sci. Rep.*, 2014, **4**, 5004.

33 K. K. Liu, C. C. Wang, C. L. Cheng and J. I. Chao, *Biomaterials*, 2009, **30**, 4249–4259.

34 J. S. Donner, S. A. Thompson, M. P. Kreuzer, G. Baffou and R. Quidant, *Nano Lett.*, 2012, **12**, 2107–2112.

35 J. S. Donner, S. A. Thompson, C. Alonso-Ortega, J. Morales, L. G. Rico, S. I. Santos and R. Quidant, *ACS Nano*, 2013, **7**, 8666–8672.

36 S. Kiyonaka, T. Kajimoto, R. Sakaguchi, D. Shinmi, M. Omatsu-Kanbe, H. Matsuura, H. Imamura, T. Yoshizaki, I. Hamachi, T. Morii and Y. Mori, *Nat. Methods*, 2013, **10**, 1232–1238.

37 K. Okabe, N. Inada, C. Gota, Y. Harada, T. Funatsu and S. Uchiyama, *Nat. Commun.*, 2012, **3**, 705.

38 T. Tsuji, K. Ikado, H. Koizumi, S. Uchiyama and K. Kajimoto, *Sci. Rep.*, 2017, **7**, 12889.

39 T. Takebe, K. Sekine, M. Enomura, H. Koike, M. Kimura, T. Ogaeri, R. R. Zhang, Y. Ueno, Y. W. Zheng, N. Koike, S. Aoyama, Y. Adachi and H. Taniguchi, *Nature*, 2013, **499**, 481–484.

40 Q. Ding and C. A. Cowan, *Cell Res.*, 2013, **23**, 1242–1243.